Surface-Enhanced Resonance Raman Spectroscopic Studies of the Cd(II) and Hg(II) Complexes of 1-(2-Pyridylazo)-2-naphthol Adsorbed on Silver Sol

Trevor J. Dines* and Hong Wu

Division of Physical and Inorganic Chemistry, Carnelley Building, University of Dundee, Dundee DD1 4HN, U.K.

Received: May 12, 2004; In Final Form: June 30, 2004

The resonance Raman (RR) and surface-enhanced resonance Raman (SERRS) spectra of $M(PAN)_2$ complexes (M = Cd and Hg, PAN^- = 1-(2-pyridylazo)-2-naphtholate) are reported and assigned, and the nature of the adsorbed species are determined. Vibrational assignments are supported by ab initio calculations at the B3-LYP/LanL2DZ level. There is clear evidence for chemisorption of these complexes on the silver surface, which gives rise to substantial alteration of the Raman spectrum. Comparison of the variation of Raman intensities with excitation wavelength for the RR and SERRS spectra indicates that there is a modification of electronic structure upon adsorption. Alterations in the Raman spectrum upon adsorption were successfully interpreted by ab initio calculations of the interaction of $M(PAN)_2$ complexes with surface silver atoms binding through the azo group α-nitrogen atoms.

Introduction

Surface-enhanced Raman scattering (SERS) spectroscopy is rapidly becoming established as a sensitive analytical technique and for studies of the adsorption of molecules on metal surfaces in aqueous media.[1,2] Silver and gold hydrosols and organosols have proved to be popular substrates for analytical SERS experiments, although careful control of particle size is essential. In an investigation of the possible use of SERS for the detection of toxic metal ions in the aquatic environment we have examined the SERS spectra of various complexes of cadmium, mercury, and lead. To further increase sensitivity we have focused attention on complexes which display intense electronic absorption in the visible region, thereby yielding resonance-enhanced Raman spectra. The combination of resonance- and surface-enhancement (SERRS) is known to provide an overall Raman intensity enhancement in excess of 10^{12} in favorable cases.[3,4] For optimum SERRS signal the energy of the resonant electronic transition should closely match the surface plasmon resonance of the substrate. This requirement dictates that, for partially aggregated silver sols, the adsorbate should possess an intense electronic absorption band in the 450−550 nm region. This condition is fulfilled by the metal complexes formed with 1-(2-pyridylazo)-2-naphthol (HPAN), which is employed as an analytical reagent for the determination of several metal ions. Upon loss of a proton it may act as a bidentate or tridentate ligand, although the mode of coordination and stoichiometry depend on the metal ion and reaction conditions, especially pH.[5]

The resonance Raman (RR) spectra of HPAN and some of its metal complexes have been assigned,[5−7] and in an earlier paper we reported a RR and SERRS investigation of the $Pb(PAN)_2$ complex.[8] An important feature of the SERRS spectrum was that there were a number of differences from the solution RR spectrum, in terms of band wavenumber shifts and a substantial alteration of relative band intensities, indicating a strong chemical interaction with the silver surface. We now present the results obtained from a RR and SERRS study of the cadmium(II) and mercury(II) complexes with PAN^-. The structure of an $M(PAN)_2$ complex with tridentate coordination is shown in Figure 1. Although previous studies of PAN complexes have reported vibrational assignments, these are incomplete, and we have therefore undertaken ab initio calculations of the structures and vibrational spectra of the Cd(II) and Hg(II) complexes at the B3-LYP/LanL2DZ level. These calculations have also proved essential to the interpretation of changes that occur in the spectra upon adsorption on a silver surface.

Experimental Section

All chemicals were of high purity or analytical grade and used without further purification. A 0.1% w/v aqueous solution of cadmium(II) chloride (100 cm^3) was adjusted to pH 5−6 with ethanoic acid. A solution of 0.2 g of HPAN in 100 cm^3 methanol was mixed with the solution of cadmium chloride, and a red colored precipitate was produced. The precipitate of $Cd(PAN)_2$ was filtered, recrystallized from carbon tetrachloride, dried, and stored in a desiccator. An aqueous solution containing 0.5 g of mercury(II) chloride (100 cm^3), previously adjusted to pH 3.5−4.5 with ethanoic acid, was added to 0.2 g of HPAN in methanol (100 cm^3), and the mixture was shaken for 3 min. A dark red colored precipitate of $Hg(PAN)_2$ was produced, which was extracted several times with carbon tetrachloride (100 cm^3). The combined extract was evaporated to dryness, and the residue was recrystallized from carbon tetrachloride, dried, and stored in a desiccator.

Silver sols were prepared by the method of Creighton et al.[9] using solutions prepared in triple-distilled water. Glassware for the sol preparations was soaked in 50% nitric acid and rinsed several times with deionized water and finally with triple-distilled water. Samples for SERRS measurements were obtained by mixing 1 cm^3 Ag sol with 1 cm^3 of either $Cd(PAN)_2$ or $Hg(PAN)_2$ in ethanol. As noted previously[4] it was necessary to induce partial sol coagulation to increase SERS intensity, by addition of 0.1 mol dm^{-3} KCl.

* Corresponding author e-mail: t.j.dines@dundee.ac.uk.

10.1021/jp047968s CCC: $27.50
Published on Web 08/10/2004

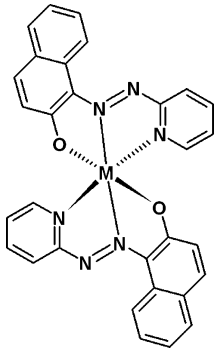

Figure 1. The structure of the $M(PAN)_2$ complexes.

Raman spectra were recorded on a Spex 1403 spectrometer controlled by a DM3000 data station, using argon ion laser excitation in the range 457.9−528.7 nm (Coherent Radiation Innova 90−6). RR spectra were obtained from 10^{-3} mol dm^{-3} solutions of $Cd(PAN)_2$ or $Hg(PAN)_2$ in ethanol, contained in a capillary tube, and illuminated in the 90° scattering geometry. For SERRS measurements samples were illuminated in the 180° scattering geometry in static glass cells. All spectra were recorded with a spectral slit width in the range 2−3 cm^{-1} and corrected for the spectral sensitivity of the spectrometer. The spectrometer calibration was checked by reference to the neon emission spectrum.

UV−visible absorption spectra were measured on a Perkin-Elmer Lambda 16 spectrophotometer.

Computational Details

There have been no published crystallographic studies of either $Cd(PAN)_2$ or $Hg(PAN)_2$ although there have been for other PAN^- complexes, e.g. 1-(2-pyridylazo)-2-naphtholato-N, N″,O)−(nitrato-O)copper(II).[10] In this complex, as in $Cd(PAN)_2$ and $Hg(PAN)_2$, PAN^- is a tridentate ligand, binding to the metal cation through the pyridyl nitrogen atom, the azo group β nitrogen atom, and the oxygen atom. It is reasonable to expect that the tridentate $M(PAN)_2$ complexes, which are six-coordinate, possess C_2 symmetry. Ab initio calculations were performed using the *Gaussian 98* program,[11] initially at the HF-SCF level and subsequently using the hybrid SCF-DFT method B3-LYP. The latter incorporates Becke's three parameter hybrid functional[12] and the Lee, Yang, and Parr correlation functional[13] and generally gives superior results to HF-SCF calculations, which neglect the effects of electron correlation. All calculations were performed with the LanL2DZ basis set, which employs Dunning−Huzinaga double-ζ (DZ) basis functions[14] on first row elements and Los Alamos effective core potential with DZ functions on heavier atoms.[15] The optimized geometry for $Cd(PAN)_2$ is shown in Figure 2, and the calculated bond lengths and interbond angles for both complexes are listed in Table 1, where they are compared with experimental data reported for 1-(2-pyridylazo)-2-naphtholato-N, N″,O)−(nitrato-O)copper-(II)[10] and calculations of the structure of $Cd(PAN)_2$ interacting with silver atoms (vide infra). The atom numbering scheme is given in Figure 3.

The calculated geometries of the Cd(II) and Hg(II) complexes are very similar, except for the metal−ligand bond distances and the θ(NMN) and θ(NMO) angles at the metal center. Comparison with the experimental data for the Cu(II) complex indicates that, apart from the metal−ligand distances and angles, the geometries are fairly similar, although the computed bond distances are mostly ca. 0.01−0.02 Å larger, which is attributable to the lack of polarization functions in the basis set (especially *d* functions on C, N, and O atoms). Bond angles are mostly within 1°, apart from those at the metal center. It is significant that for both the experimental geometry of the Cu(II) complex and the computed geometries for the Cd(II) and Hg(II) complexes, the NN distance is larger than expected for a double bond and the CO distance is shorter than that for a single bond. The neutral protonated species, HPAN, exhibits azo-hydrazo tautomerism, thus in these metal complexes it appears that the structure is midway between azo- and hydrazo-forms.

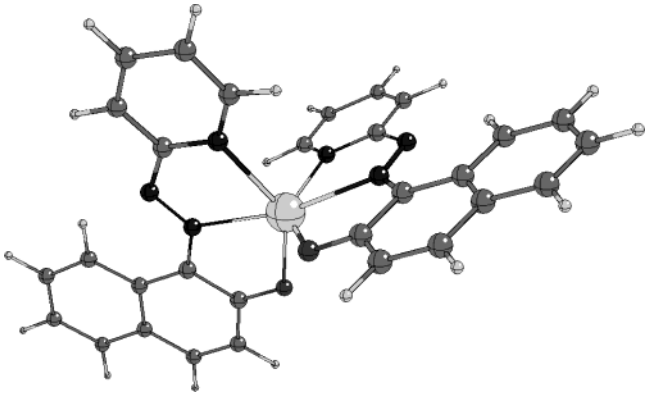

Figure 2. Optimized molecular geometry of $Cd(PAN)_2$ calculated at the B3LYP/LanL2DZ level.

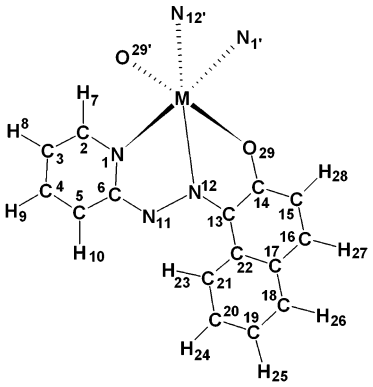

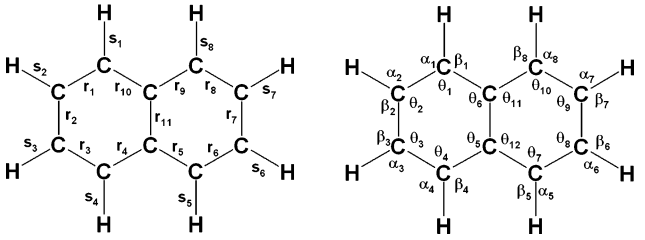

Figure 3. Atom numbering scheme and definition of symmetry coordinates for the naphthalene ring.

The vibrational spectrum of each complex was calculated at the optimized geometry using the B3-LYP method with the LanL2DZ basis set; the 171 normal modes are classified as follows:

$$\Gamma_{3N-6} = 86a + 85b$$

All of these are active in both IR and Raman, although it is expected that only the modes of *a* symmetry are likely to give rise to strong bands in the RR spectra, unless there is a change of molecular symmetry in the resonant excited state, consistent with the A-term RR scattering mechanism.[16] It is possible, however, that in the SERRS spectra some *b* modes may yield strong bands due to either the operation of surface selection

TABLE 1: Calculated Molecular Geometry for $Cd(PAN)_2$ and $Hg(PAN)_2$ in the Free State and $Cd(PAN)_2$ Complexed to Two Silver Atoms, Compared with Experimental Data for a PAN Complex[a]

	expt.[10]	$Cd(PAN)_2$	$Cd(PAN)_2\cdots 2Ag^0$	$Hg(PAN)_2$		expt.[10]	$Cd(PAN)_2$	$Cd(PAN)_2\cdots 2Ag^0$	$Hg(PAN)_2$
r(N1C6)	1.355	1.367	1.365	1.364	θ(C4C3H8)	120.5	121.7	121.7	121.7
r(N1M)	1.980	2.389	2.405	2.474	θ(C3C4H9)	120.3	120.4	120.4	120.4
r(C2N1)	1.338	1.356	1.360	1.355	θ(C4C5H10)	121.0	122.3	121.6	122.3
r(C3C2)	1.380	1.403	1.399	1.403	θ(C4C5C6)	118.5	119.3	119.4	119.3
r(C3C4)	1.378	1.413	1.417	1.414	θ(C5C4H9)	120.4	120.2	120.1	120.2
r(C4C5)	1.386	1.399	1.396	1.399	θ(H10C5C6)	120.5	118.4	119.0	118.4
r(C5H10)	0.959	1.084	1.086	1.085	θ(C5C6N11)	119.1	116.6	118.4	116.2
r(C5C6)	1.386	1.418	1.421	1.419	θ(C6N11N12)	110.3	114.1	113.8	115.2
r(C6N11)	1.408	1.413	1.416	1.414	θ(N11N12C13)	125.4	123.0	122.4	122.8
r(H7C2)	0.958	1.086	1.086	1.086	θ(N11N12M)	119.8	120.2	121.0	120.0
r(H8C3)	0.959	1.085	1.085	1.085	θ(N12C13C22)	128.3	127.8	127.9	127.3
r(H9C4)	0.960	1.087	1.087	1.087	θ(N12C13C14)	110.4	112.1	112.3	112.8
r(N11N12)	1.297	1.323	1.351	1.321	θ(C13N12M)	114.8	116.7	116.5	117.2
r(N12C13)	1.354	1.363	1.362	1.364	θ(C22C13C14)	121.4	120.1	119.8	119.9
r(C13C22)	1.455	1.465	1.465	1.468	θ(C13C22C21)	123.9	123.9	123.8	123.9
r(C13C14)	1.434	1.473	1.474	1.473	θ(C13C22C17)	117.3	118.4	118.5	118.6
r(C14C15)	1.422	1.451	1.444	1.452	θ(C13C14C15)	118.5	118.3	118.2	118.3
r(C15H28)	0.959	1.086	1.086	1.085	θ(C13C14O29)	120.8	122.6	121.8	123.5
r(C15C16)	1.348	1.369	1.375	1.368	θ(C14C15H28)	119.5	116.5	116.5	116.3
r(C16H27)	0.960	1.089	1.089	1.089	θ(C14C15C16)	120.6	121.1	121.4	121.3
r(C17C18)	1.406	1.417	1.422	1.418	θ(C15C14O29)	120.7	119.0	120.0	118.2
r(C17C16)	1.446	1.448	1.444	1.448	θ(H28C15C16)	119.9	122.4	122.1	122.4
r(C18H26)	0.960	1.088	1.088	1.088	θ(C15C16H27)	118.9	119.9	120.0	120.0
r(C19C18)	1.377	1.398	1.396	1.398	θ(C15C16C17)	122.5	122.1	121.8	122.0
r(C19H25)	0.961	1.087	1.087	1.087	θ(H27C16C17)	118.6	117.9	118.1	118.0
r(C20C19)	1.382	1.413	1.417	1.413	θ(C18C17C16)	120.4	119.7	120.2	119.6
r(C21C20)	1.393	1.401	1.399	1.401	θ(C17C18H26)	119.4	118.8	118.6	118.8
r(C21C22)	1.412	1.425	1.432	1.425	θ(C17C18C19)	120.6	121.0	121.3	121.0
r(C22C17)	1.413	1.438	1.441	1.438	θ(C18C17C22)	119.9	120.3	119.9	120.4
r(H23C21)	0.961	1.080	1.083	1.080	θ(C16C17C22)	119.6	120.0	119.9	120.0
r(H24C20)	0.960	1.088	1.088	1.088	θ(H26C18C19)	120.1	120.2	120.1	120.3
r(O29C14)	1.296	1.301	1.307	1.301	θ(C18C19H25)	120.0	120.5	120.5	120.5
r(MO29)	1.947	2.270	2.271	2.369	θ(C18C19C20)	119.7	119.1	119.2	119.0
r(MN12)	1.951	2.415	2.388	2.505	θ(H25C19C20)	120.2	120.4	120.3	120.4
r(N11Ag)	2.315				θ(C19C20C21)	121.6	121.0	120.7	121.0
θ(C6N1M)	111.6	115.1	115.9	115.5	θ(C19C20H24)	119.2	119.7	119.9	119.7
θ(C6N1C2)	118.7	119.5	119.5	119.9	θ(C20C21C22)	119.4	120.9	121.3	121.0
θ(N1C6C5)	122.1	120.9	120.8	120.7	θ(C20C21H23)	120.6	120.6	119.7	120.5
θ(N1C6N11)	118.8	122.5	120.8	123.1	θ(C21C20H24)	119.2	119.3	119.4	119.3
θ(MN1C2)	129.7	125.4	124.1	124.7	θ(C21C22C17)	118.7	117.7	117.5	117.5
θ(N1MO29)	162.0	138.1	137.5	134.1	θ(C22C21H23)	119.9	118.5	118.9	118.4
θ(N1MN12)	79.4	68.1	67.4	66.2	θ(C14O29M)	111.4	118.4	117.8	118.5
θ(N1MN1′)		95.9	98.3	98.6	θ(O29MN12)	82.7	70.1	70.3	68.0
θ(N1MN12′)		103.3	100.7	103.3	θ(O29MN1′)	94.8	93.7	93.9	
θ(N1MO29′)		94.8	93.7	93.9	θ(O29MN12′)	118.2	121.5	122.1	
θ(N1C2C3)	122.1	122.7	122.9	122.5	θ(O29MO29′)	103.7	104.5	108.3	
θ(N1C2H7)	118.5	116.3	116.0	116.4	θ(N12MN1′)	103.3	100.7	103.3	
θ(C2C3C4)	119.3	118.2	118.0	118.2	θ(N12MN12′)	167.7	162.6	164.7	
θ(C3C2H7)	119.3	121.0	121.2	121.1	θ(N12MO29′)	118.2	121.5	122.1	
θ(C2C3H8)	120.2	120.2	120.3	120.2	θ(C6N11Ag)	115.1			
θ(C3C4C5)	119.3	119.4	119.5	119.4	θ(AgN11N12)	113.9			

[a] Bond distances in Ångstrom units and interbond angles in degrees.

rules[17] or lowering in symmetry as a result of chemisorption at the silver surface.

For computation of the potential energy distributions associated with the vibrational modes, the Cartesian force constants obtained from the Gaussian 98 output were converted to force constants expressed in terms of internal coordinates. The neglect of electron correlation in the HF-SCF method is a major cause of error which is to a large extent eliminated in the hybrid SCF-DFT calculations. However, in both methods it is the harmonic vibrational wavenumbers that are obtained, and a good fit would not be expected for modes which are especially anharmonic, which is usually the case for vibrations involving motion of hydrogen atoms. For proper comparison with experimental spectra scaling of the calculated force field is necessary even with the B3-LYP method. Scaling factors were applied to the force constants before input to a normal coordinate analysis program derived from those of Schachtschneider.[18] Scaling of force constants, expressed in internal coordinates, was applied according to the following formula

$$f_{ij}^{scaled} = f_{ij}^{calc}\sqrt{s_i s_j}$$

where s_i and s_j are scale factors relating to internal coordinates i and j, following the Pulay SQM-FF method.[19] In these calculations the scale factors were 0.91 for CH stretching, 0.95 for CH in-plane and out-of-plane deformation, 1.00 for C═O stretching, 0.965 for NN stretching, and 0.955 for all other coordinates. These were chosen to give the best fit to the experimental data.

Symmetry-adapted linear combinations of internal coordinates were constructed according to the symmetry elements of the C_2 point group. Wilson symmetry coordinates were used for

the CC stretching and in-plane and out-of-plane ring deformations of the pyridine rings.[20] Symmetry-adapted coordinates were devised for the skeletal modes of the naphthalene rings in order to remove redundancies associated with vibrations of these rings. These were designed to match the naphthalene normal modes as closely as possible; they have not previously been published and are listed in Table 2. The scaled vibrational wavenumbers from B3-LYP/DZ calculation are listed in Table 3 for the Cd(PAN)$_2$ free complex and with interaction with silver atoms, together with assignments based upon potential energy distributions (peds), for the vibrations of a symmetry only. The results obtained for Hg(PAN)$_2$, in terms of both the structure and vibrational spectrum, are sufficiently similar to those of Cd(PAN)$_2$ that additional tables giving those data were considered unnecessary. Detailed examination of the SERRS spectra (vide infra) suggested that the most likely site for coordination to silver would be through the azo group α-nitrogen atom. Accordingly, we calculated the structure and spectra of both complexes with attachment of silver atoms to the α-nitrogen atoms of both ligands. Although it is likely that the complex binds to the silver surface through only one ligand, this enabled the C_2 symmetry to be preserved in the calculation. These calculations indicated a small degree of charge transfer from metal complex to silver, giving a charge of +0.132 on each silver atom and −0.736 on the Cd(II) complex and a charge of +0.150 on each silver atom and −0.700 on the Hg(II) complex. The data in Table 1 reveal that some geometric changes occur upon interaction with silver. The most notable difference is an increase in the NN distance by 0.028 Å. Pyridine ring and CN bond distances are largely unaffected although naphthalene ring bond distances are altered by up to 0.05 Å, the M−N1 distance increases by 0.016 Å, the M−N12 distance decreases by 0.027 Å, but the M−O distance remains unchanged. B3-LYP/LanL2DZ calculations were also carried out for the Cd(II) and Hg(II) complexes interacting, at the azo group α-nitrogen atoms, with either two Ag^+ ions or one Ag^+ ion and one neutral Ag atom. However, the results gave a much less satisfactory fit to the band shifts observed in the SERRS spectra.

Electronic transitions were determined from excited-state calculations using the time-dependent DFT method (B3-LYP/DZ),[21] for which the results are listed in Table 4. Diagrams of the frontier orbitals involved in these transitions are shown in Figure 4. Several electronic transitions are predicted in the visible region, although the four lowest energy ones have very low oscillator strengths. The remaining four may be grouped into two pairs, each consisting of ^{1}A←^{1}A and ^{1}B←^{1}A transitions which are very close together. The pair predicted at around 475−478 nm are predicted to have comparable intensity; the orbitals involved in these transitions are the two highest occupied ones (nos. 134 and 135) and the two lowest unoccupied ones (136 and 137). Orbitals 134 and 135 are of similar type, representing symmetric (134) and antisymmetric (135) combinations of the contributions from the two ligands, with no contribution from metal orbitals. In these two π orbitals electron density is mainly localized on the azo α-nitrogen, the naphthalene α-carbon, and the oxygen atoms, with only small contributions from the pyridine and naphthalene rings. Orbitals 136 and 137 also represent symmetric and antisymmetric combinations. In this case electron density is localized on the azo group and also the other ligand atoms, and these orbitals may be regarded as of azo π^* type. This pair of transitions are therefore of HOMO−LUMO $\pi-\pi^*$ character and largely uninfluenced by the metal cation. They may both contribute to the A-term RR scattering mechanism, and there is expected to be no destructive interference because they contribute to different transition polarizability components.

At higher energy (around 406 nm) there are another pair of ^{1}A←^{1}A and ^{1}B←^{1}A transitions, of which the ^{1}B←^{1}A is predicted to be more intense but much less intense than the lower energy transitions. These transitions involve promotion of electrons

TABLE 2: Definitions of Naphthalene Ring Symmetry-Adapted Coordinates[a]

A_g

$N_{N1} = s_1 + s_4 + s_5 + s_8$

$N_2 = s_2 + s_3 + s_6 + s_7$

$N_3 = r_1 + r_3 + r_6 + r_8$

$N_4 = r_4 + r_5 + r_9 + r_{10}$

$N_5 = r_2 + r_7$

$N_6 = r_{11}$

$N_7 = \phi_1 + \phi_4 + \phi_5 + \phi_8$

$N_8 = \phi_2 + \phi_3 + \phi_6 + \phi_7$

$N_9 = -2\theta_1 + \theta_2 + \theta_3 - 2\theta_4 + \theta_5 + \theta_6 - 2\theta_7 + \theta_8 + \theta_9 - 2\theta_{10} + \theta_{11} + \theta_{12} =$ **[6a + 6a′]**

B_{1g}

$N_{10} = \omega_1 - \omega_4 - \omega_5 + \omega_8$

$N_{11} = \omega_2 - \omega_3 - \omega_6 + \omega_7$

$N_{12} = \tau_1 - \tau_3 + \tau_4 - \tau_{10} - \tau_6 + \tau_8 - \tau_9 + \tau_5 =$ **[16b − 16b′]**

B_{2g}

$N_{13} = \omega_1 + \omega_4 - \omega_5 - \omega_8$

$N_{14} = \omega_2 + \omega_3 - \omega_6 - \omega_7$

$N_{15} = \tau_1 - \tau_2 + \tau_3 - \tau_4 + \tau_{11} - \tau_{10} - \tau_6 + \tau_7 - \tau_8 + \tau_9 - \tau_{11'} + \tau_5 =$ **[4 − 4′]**

$N_{16} = -\tau_1 + 2\tau_2 - \tau_3 - \tau_4 + 2\tau_{11} - \tau_{10} + \tau_6 - 2\tau_7 + \tau_8 + \tau_9 - 2\tau_{11'} + \tau_5 =$ **[16a − 16a′]**

B_{3g}

$N_{17} = s_1 - s_4 + s_5 - s_8$

$N_{18} = s_2 - s_3 + s_6 - s_7$

$N_{19} = r_1 - r_3 + r_6 - r_8$

$N_{20} = r_4 - r_5 + r_9 - r_{10}$

$N_{21} = \phi_1 - \phi_4 + \phi_5 - \phi_8$

$N_{22} = \phi_2 - \phi_3 + \phi_6 - \phi_7$

$N_{23} = \theta_2 - \theta_3 + \theta_5 - \theta_6 + \theta_8 - \theta_9 + \theta_{11} - \theta_{12} =$ **[6b + 6b′]**

$N_{24} = -\theta_1 + \theta_2 - \theta_3 + \theta_4 - \theta_5 + \theta_6 - \theta_7 + \theta_8 - \theta_9 + \theta_{10} - \theta_{11} + \theta_{12} =$ **[12 + 12′]**

A_u

$N_{25} = \omega_1 + \omega_4 + \omega_5 + \omega_8$

$N_{26} = \omega_2 + \omega_3 + \omega_6 + \omega_7$

$N_{27} = \tau_1 - \tau_2 + \tau_3 - \tau_4 + \tau_{11} - \tau_{10} + \tau_6 - \tau_7 + \tau_8 - \tau_9 + \tau_{11'} - \tau_5 =$ **[4 + 4′]**

$N_{28} = -\tau_1 + 2\tau_2 - \tau_3 - \tau_4 + 2\tau_{11} - \tau_{10} - \tau_6 + 2\tau_7 - \tau_8 - \tau_9 + 2\tau_{11'} - \tau_5 =$ **[16a + 16a′]**

B_{1u}

$N_{29} = s_1 - s_4 - s_5 + s_8$

$N_{30} = s_2 - s_3 - s_6 + s_7$

$N_{31} = r_1 - r_3 - r_6 + r_8$

$N_{32} = r_4 + r_5 - r_9 - r_{10}$

$N_{33} = \phi_1 - \phi_4 - \phi_5 + \phi_8$

$N_{34} = \phi_2 - \phi_3 - \phi_6 + \phi_7$

$N_{35} = \theta_2 - \theta_3 + \theta_5 - \theta_6 - \theta_8 + \theta_9 - \theta_{11} + \theta_{12} =$ **[6b − 6b′]**

$N_{36} = -\theta_1 + \theta_2 - \theta_3 + \theta_4 - \theta_5 + \theta_6 + \theta_7 - \theta_8 + \theta_9 - \theta_{10} + \theta_{11} - \theta_{12} =$ **[12 − 12′]**

B_{2u}

$N_{37} = s_1 + s_4 - s_5 - s_8$

$N_{38} = s_2 + s_3 - s_6 - s_7$

$N_{39} = r_1 + r_3 - r_6 - r_8$

$N_{40} = r_4 - r_5 - r_9 + r_{10}$

$N_{41} = r_2 - r_7$

$N_{42} = \phi_1 + \phi_4 - \phi_5 - \phi_8$

$N_{43} = \phi_2 + \phi_3 - \phi_6 - \phi_7$

$N_{44} = -2\theta_1 + \theta_2 + \theta_3 - 2\theta_4 + \theta_5 + \theta_6 + 2\theta_7 - \theta_8 - \theta_9 + 2\theta_{10} - \theta_{11} - \theta_{12} =$ **[6a − 6a′]**

B_{3u}

$N_{45} = \omega_1 - \omega_4 + \omega_5 - \omega_8$

$N_{46} = \omega_2 - \omega_3 + \omega_6 - \omega_7$

$N_{47} = \tau_1 - \tau_3 + \tau_4 - \tau_{10} + \tau_6 - \tau_8 + \tau_9 - \tau_5 =$ **[16b + 16b′]**

$N_{48} = \tau_{10'} - \tau_{9'} + \tau_{5'} - \tau_{4'}$

[a] Refers to combinations (±) of Wilson coordinates for benzene.

TABLE 3: Calculated Molecular Vibrations and Assignments (peds) for $Cd(PAN)_2$ Free Molecule and Interaction with Ag^0

3125	ν(C21H23) (98)	3102	ν(C21H23) (92)
3104	ν(C3H8) (30), ν(C4H9) (15), ν(C5H10) (49)	3100	ν(C2H7) (12), ν(C3H8) (71), ν(C4H9) (13)
3095	ν(C3H8) (49), ν(C5H10) (42)	3086	ν(C15H28) (91)
3089	ν(C15H28) (92)	3078	ν(C4H9) (36), ν(C5H10) (48)
3076	ν(C18H26) (12), ν(C19H25) (66), ν(C20H24) (21)	3075	ν(C18H26) (12), ν(C19H25) (66), ν(C20H24) (17)
3069	ν(C2H7) (62), ν(C4H9) (33)	3067	ν(C2H7) (74), ν(C3H8) (13), ν(C5H10) (10)
3063	ν(C2H7) (25), ν(C3H8) (19), ν(C4H9) (51)	3059	ν(C4H9) (48), ν(C5H10) (39)
3052	ν(C18H26) (27), ν(C20H24) (65)	3051	ν(C18H26) (19), ν(C20H24) (64)
3043	ν(C16H27) (67), ν(C18H26) (12), ν(C19H25) (10)	3044	ν(C16H27) (78)
3039	ν(C16H27) (25), ν(C18H26) (49), ν(C19H25) (18)	3039	ν(C16H27) (47), ν(C18H26) (11), ν(C19H25) (18)
1624	N_3 (13), N_9 (18), N_{19} (25), N_{20} (18)	1606	N_{19} (24), N_{20} (21)
1607	N_{20} (10), N_{31} (35)	1599	S_{8b} (14), N_3 (13), N_{31} (27)
1602	S_{8b} (67)	1596	S_{8b} (50)
1567	S_{8a} (70)	1558	S_{8a} (72)
1551	N_5 (12), N_6 (13), N_{41} (12)	1537	N_5 (11), N_6 (11), N_{41} (13)
1522	ν(CO) (33), N_{40} (10)	1507	ν(CO) (23), N_{40} (11), N_{41} (12)
1479	ν(CO) (14), δ_{ip}(C18H26) (15), δ_{ip}(C21H23) (16)	1467	ν(CO) (11), S_{19b} (10), δ_{ip}(C2H7) (13), δ_{ip}(C18H26) (11), δ_{ip}(C21H23) (12)
1466	S_{19b} (21), δ_{ip}(C2H7) (30), δ_{ip}(C5H10) (13)	1458	S_{19b} (15), δ_{ip}(C2H7) (24), δ_{ip}(C5H10) (11)
1449	N_{20} (15), δ_{ip}(C19H25) (12), δ_{ip}(C20H24) (15)	1438	N_{20} (13), δ_{ip}(C20H24) (11)
1434	S_{19a} (29), δ_{ip}(C3H8) (26), δ_{ip}(C4H9) (19)	1428	S_{19a} (24), δ_{ip}(C3H8) (22), δ_{ip}(C4H9) (16)
1409	δ_{ip}(C15H28) (10), δ_{ip}(C16H27) (18), δ_{ip}(C19H25) (11)	1404	ν(C13N12) (10), δ_{ip}(C16H27) (12)
1380	N_{39} (18), ν(C13N12) (24)	1369	N_4 (14), N_{39} (24), ν(C13N12) (12)
1358	N_3 (14), N_4 (12), N_6 (17)	1353	S_{14} (13), N_3 (10), N_6 (10), ν(C13N12) (15), δ_{ip}(C16H27) (11)
1337	ν(NN) (29), S_{14} (19)	1327	S_{14} (50)
1326	N_{40} (14), δ_{ip}(C21H23) (12)	1321	δ_{ip}(C15H28) (12)
1317	ν(NN) (11), S_{14} (27), δ_{ip}(C5H10) (13)	1298	S_{14} (10), δ_{ip}(C2H7) (21), δ_{ip}(C5H10) (14)
1295	S_{14} (33), δ_{ip}(C2H7) (21), δ_{ip}(C5H10) (11)	1292	ν(NN) (12), N_{20} (10), δ_{ip}(C21H23) (16)
1263	ν(NN) (12), δ_{ip}(C18H26) (21), δ_{ip}(C21H23) (16)	1248	ν(C6N11) (32), S_{12} (11)
1245	ν(C6N11) (23)	1235	ν(NN) (17), N_{32} (15), ν(C13N12) (10), δ_{ip}(C18H26) (16), δ_{ip}(C21H23) (10)
1225	N_{40} (35), δ_{ip}(C16H27) (18)	1226	N_{40} (38), δ_{ip}(C16H27) (27)
1178	δ_{ip}(C19H25) (28), δ_{ip}(C20H24) (33), δ_{ip}(C21H23) (10)	1177	δ_{ip}(C18H26) (11), δ_{ip}(C19H25) (32), δ_{ip}(C20H24) (31)
1167	δ_{ip}(C3H8) (13), δ_{ip}(C4H9) (21)	1164	S_{8a} (10), δ_{ip}(C3H8) (29), δ_{ip}(C4H9) (31), δ_{ip}(C5H10) (20)
1160	δ_{ip}(C3H8) (19), δ_{ip}(C4H9) (10), δ_{ip}(C5H10) (14)	1143	ν(NN) (11), N_{19} (14), δ_{ip}(C15H28) (35), δ_{ip}(C16H27) (14)
1144	N_{19} (31), δ_{ip}(C15H28) (20), δ_{ip}(C16H27) (14)	1140	ν(NN) (15), N_{19} (18), δ_{ip}(C19H25) (12), δ_{ip}(C20H24) (10)
1110	S_{19a} (25), δ_{ip}(C3H8) (18), δ_{ip}(C5H10) (12)	1112	S_{19a} (28), δ_{ip}(C3H8) (22), δ_{ip}(C5H10) (10)
1086	N_{24} (11), N_{32} (10), N_{36} (18)	1074	ν(NN) (13), N_{24} (14), N_{36} (15)
1049	N_3 (13), N_5 (32)	1046	N_3 (13), N_5 (33)
1037	S_1 (10), S_{19b} (55), δ_{ip}(C5H10) (13)	1036	S_1 (11), S_{19b} (53), δ_{ip}(C5H10) (11)
1026	δ_{op}(C19H25) (12), δ_{op}(C20H24) (48), δ_{op}(C21H23) (57)	1013	S_1 (21), S_{12} (37), δ_{op}(C21H23) (11)
1017	S_1 (29), S_{12} (42)	1009	S_1 (12), S_{12} (11), δ_{op}(C19H25) (17), δ_{op}(C20H24) (34), δ_{op}(C21H23) (33)
1013	δ_{op}(C3H8) (20), δ_{op}(C4H9) (65), δ_{op}(C5H10) (29)	1002	δ_{op}(C3H8) (24), δ_{op}(C4H9) (61), δ_{op}(C5H10) (23)
1010	δ_{op}(C15H28) (37), δ_{op}(C16H27) (62), δ_{op}(C18H25) (10)	1000	S_1 (13), N_{39} (14), N_{41} (16)
1002	S_1 (20), N_{39} (18), N_{41} (20)	992	δ_{op}(C15H28) (26), δ_{op}(C18H26) (38), δ_{op}(C19H25) (14), δ_{op}(C21H23) (12)
984	δ_{op}(C15H28) (10), δ_{op}(C18H26) (35), δ_{op}(C19H25) (45), δ_{op}(C21H23) (16)	976	δ_{op}(C15H28) (23), δ_{op}(C16H27) (18), δ_{op}(C18H26) (25), δ_{op}(C19H25) (28), δ_{op}(C21H23) (16)
977	δ_{op}(C2H7) (72), δ_{op}(C3H8) (22), δ_{op}(C5H10) (11)	972	δ_{op}(C2H7) (70), δ_{op}(C3H8) (17), δ_{op}(C4H9) (11), δ_{op}(C5H10) (11)
913	δ_{op}(C18H26) (35), δ_{op}(C20H24) (23), δ_{op}(C21H23) (20)	899	δ_{op}(C18H26) (29), δ_{op}(C19H25) (12), δ_{op}(C10H24) (18), δ_{op}(C21H23) (21)
900	δ_{op}(C2H7) (19), δ_{op}(C3H8) (19), δ_{op}(C4H9) (11),	887	N_{24} (31), δ(C6N11N12) (14), δ_{op}(C5H10) (51)
890	N_{24} (37), δ(C6N11N12) (14)	883	δ_{op}(C2H7) (10), δ_{op}(C3H8) (25), δ_{op}(C5H10) (50)
856	δ_{op}(CO) (21), δ_{op}(C15H28) (40), δ_{op}(C16H27) (26)	855	S_1 (13), N_{24} (12), ν(C6N11) (21)
853	S_1 (13), N_{24} (19), ν(C6N11) (14)	843	δ_{op}(CO) (13), δ_{op}(C15H28) (29), δ_{op}(C16H27) (25)
819	N_{15} (57), δ_{op}(CO) (11), δ_{op}(C13N12) (12)	805	N_{15} (65), δ_{op}(CO) (12), δ_{op}(C13N12) (11)
797	S_4 (22), N_{15} (10), δ_{op}(C3H8) (25), δ_{op}(C6N11) (24)	788	S_4 (25), δ_{op}(C3H8) (26), δ_{op}(C6N11) (24)
779	δ_{op}(C18H26) (19), δ_{op}(C19H25) (35), δ_{op}(C20H24) (25)	770	δ_{op}(C18H26) (18), δ_{op}(C19H25) (32), δ_{op}(C20H24) (27)
763	S_4 (54), δ_{op}(C3H8) (15), δ_{op}(C4H9) (14), δ_{op}(C5H10) (12)	756	S_4 (53), δ_{op}(C3H8) (14), δ_{op}(C4H9) (14), δ_{op}(C5H10) (14)
746	N_4 (12), N_{32} (11), N_{35} (10), N_{36} (23)	743	N_4 (11), N_{32} (12), N_{35} (11), N_{36} (25)
731	N_6 (10), N_{36} (14)	728	N_6 (12), N_{36} (10)
703	N_{15} (13), N_{27} (46), δ_{op}(CO) (22)	694	N_{27} (44), δ_{op}(CO) (17)
656	S_{6a} (49), N_{35} (14)	655	S_{6a} (50), N_{35} (13)
645	S_{6a} (17), S_{6b} (38), N_{35} (10)	645	S_{6a} (16), S_{6b} (40)
616	S_{6b} (11), N_{44} (16), δ_{ip}(CO) (22)	618	S_{6b} (12), N_{44} (14), δ_{ip}(CO) (20)
588	N_{47} (23), δ_{op}(C13N12) (21), τ(C13N12) (10), τ(NN) (10)	569	N_{47} (31), δ_{op}(C13N12) (24), τ(NN) (10)
557	N_4 (10), N_{35} (29)	564	N_{35} (27)
549	N_{16} (32), N_{27} (29)	548	N_{16} (28), N_{27} (23), δ_{op}(C6N11) (23)
520	S_4 (15), S_{16a} (25), N_{47} (12), δ_{op}(C6N11) (26)	535	S_4 (11), N_{16} (11), N_{27} (13), δ_{op}(C6N11) (17)
515	N_{23} (12), δ_{ip}(C6N11) (13), δ_{ip}(CO) (16)	520	N_{23} (10), δ_{ip}(CO) (15)
492	S_{6b} (10), N_{23} (36), δ_{ip}(CO) (11)	493	N_{23} (38)
440	S_{16a} (33), S_{16b} (56)	437	N_9 (12), N_{12} (36), N_{47} (29), τ(C13N12) (10)
436	N_{12} (36), N_{47} (34)	436	S_{16a} (36), S_{16b} (60)

TABLE 3: (Continued)

436	N_{12} (36), N_{47} (34)	436	S_{16a} (36), S_{16b} (60)
433	N_4 (14), N_9 (42), N_{44} (10)	431	N_4 (13), N_9 (31), N_{44} (12)
381	N_{12} (33), N_{16} (28), τ(C13N12) (20)	395	N_{12} (31), N_{16} (18), τ(C13N12) (13), δ_{op}(AgN) (12)
351	N_{31} (11), N_{44} (18), δ_{ip}(C6N11) (16), ν(CdO) (15)	352	N_{44} (13), ν(CdO) (13)
348	N_{31} (11), N_{44} (19), δ_{ip}(C6N11) (15), ν(CdO) (14)	336	N_{16} (13), δ_{op}(CO) (13)
312	S_{16a} (21), S_{16b} (15), δ_{op}(CO) (11), τ(C13N12) (22)	292	N_{35} (12), δ_{ip}(C6N11) (11)
293	N_{35} (13), δ_{ip}(C6N11) (14)	256	N_{12} (13), N_{16} (10), N_{27} (11), N_{48} (15), τ(NN) (12)
252	N_{12} (12), N_{16} (11), N_{27} (13), N_{48} (18), τ(NN) (14)	226	δ_{ip}(C6N11) (18), ν(CdO) (17), ν(AgN) (14)
217	δ_{ip}(C6N11) (19), δ_{ip}(C13N12) (14), δ(C6N11N12) (14), ν(CdO) (17)	201	N_{28} (22), N_{48} (31), δ_{op}(C13N12) (13)
199	N_{28} (22), N_{48} (33), δ_{op}(C13N12) (14)	168	N_{28} (20), δ(pitch) (16), ν(AgN) (15)
166	ν(CdN1) (37), ν(CdO) (30)	163	ν(CdN1) (24), ν(CdO) (24)
146	N_{28} (45), δ(pitch) (15)	149	N_{28} (29), τ(C13N12) (14), ν(AgN) (18)
126	N_{47} (11), N_{48} (17), τ(C6N11) (27), δ(pitch) (25)	117	N_{47} (14), N_{48} (11), ν(AgN) (12)
100	δ_{ip}(C13N12) (12), ν(CdN1) (19), ν(CdN12) (31)	99	δ(pitch) (19), δ_{ip}(AgN) (11)
88	N_{28} (14), δ(pitch) (38)	96	ν(CdN1) (27), ν(CdN12) (20)
79	δ(C13N12N11) (13), ν(CdN1) (13), ν(CdN12) (50)	72	τ(C6N11) (17), ν(CdN12) (20), δ(pitch) (20)
54	τ(C13N12) (10), τ(NN) (27), δ(pitch) (22)	56	δ_{op}(C6N11) (10), τ(NN) (11), ν(CdN12) (15), δ_{op}(AgN) (41)
37	N_{47} (12), δ_{op}(C13N12) (10), τ(C6N11) (11), τ(NN) (12), δ(pitch) (27)	53	N_{48} (17), τ(C13N12) (21), δ(pitch) (30)
		29	τ(C6N11) (14), τ(NN) (28), δ(pitch) (13), δ_{op}(AgN) (22)

TABLE 4: Calculated Electronic Transitions for $Cd(PAN)_2$ and $Hg(PAN)_2$

	$Cd(PAN)_2$		$Hg(PAN)_2$				
no.	λ/nm	f	λ/nm	f	assignments and orbital contributions[a]		
1	555.85	0.0018	547.26	0.0006	$^1A \leftarrow {}^1A(z)$	134(a)→137(a)	−0.45617
						135(b)→136(b)	0.53742
2	555.47	0.0021	547.05	0.0008	$^1B \leftarrow {}^1A(x,y)$	134(a)→136(b)	−0.46781
						135(b)→137(a)	0.52843
3	510.49	0.0023	523.27	0.0005	$^1B \leftarrow {}^1A(x,y)$	130(a)→137(a)	−0.40207
						133(a)→136(b)	0.53533
4	510.14	0.0005	523.14	0.0005	$^1A \leftarrow {}^1A(z)$	130(b)→136(b)	−0.40646
						133(a)→137(a)	0.53272
5	478.12	0.3035	481.76	0.2597	$^1A \leftarrow {}^1A(z)$	134(a)→137(a)	0.46446
						135(b)→136(b)	0.36771
6	475.58	0.4642	477.14	0.4561	$^1B \leftarrow {}^1A(x,y)$	134(a)→136(b)	0.45091
						135(a)→137(a)	0.37782
7	405.85	0.0010	412.32	0.0019	$^1A \leftarrow {}^1A(z)$	130(b)→136(b)	0.51089
						132(b)→136(b)	0.20452
						133(a)→137(a)	0.43152
8	405.85	0.0581	412.18	0.0217	$^1B \leftarrow {}^1A(x,y)$	130(b)→137(a)	0.48060
						131(a)→136(b)	0.11758
						132(b)→137(a)	0.26500
						133(a)→136(b)	0.41320

[a] Orbital contributions calculated for $Cd(PAN)_2$; those for $Hg(PAN)_2$ are very similar.

from lower energy MOs (nos. 130 to 133) into the π^* orbitals 136 and 137. Orbitals 130 and 133 are symmetric (133) and antisymmetric (130) combinations of orbitals which have a significant σ component on the azo group, with smaller contributions from the pyridine nitrogen atoms, the oxygen atoms, and the metal cation. Orbitals 131 and 132 are symmetric (131) and antisymmetric (132) combinations which are largely of π bonding character, localized on the naphthalene rings. This pair of transitions may also contribute to the A-term RR scattering mechanism but to a much smaller extent than those at lower energy.

Time-dependent B3-LYP/LanL2DZ calculations of the electronic excited states of $Cd(PAN)_2$ and $Hg(PAN)_2$ interacting with silver atoms were also carried out. The results were very similar, and only those for $Cd(PAN)_2$ are summarized in Table 5. The interaction with silver leads to the appearance of several more transitions giving rise to absorption in the visible region. Comparison of orbital diagrams (not shown) with those of the free complex enables a number of these transitions to be correlated, showing that interaction with silver results in red-shift of the absorption spectrum with respect to that of the free complex. In particular, the $^1B \leftarrow {}^1A$ and $^1A \leftarrow {}^1A$ resonant transitions, at around 475−478 nm in the free complex, are predicted to shift to 520−530 nm, closer to the silver surface plasmon resonance. Two new orbitals are found for the interaction species, which involve contributions from the silver atoms, whose energies are between those of the HOMO and LUMO of the free complex. These become the new HOMO and LUMO, illustrated in Figure 5. They contribute significantly to the very low energy transitions (nos. 1−4), predicted to give rise to absorption in the near-IR region, and also in part to many of the transitions at higher energy, especially those in the 440−490 nm region, which have no counterpart in the free complex. For example, the two transitions at ca. 447 nm (nos. 17 and 18) are dominated by promotion of an electron from the HOMO to a π^* orbital localized on the pyridine and naphthalene rings. By contrast, the lower energy transitions (nos. 14, 15, and 16) involve electron transfer from ligand-centered orbitals to the LUMO. All of these transitions may be expected to contribute to RR enhancement for excitation in this region and lead to alterations in relative band intensities as well as significant shifts in band wavenumber positions.

Results

Electronic Absorption Spectra. The electronic absorption spectra of $Cd(PAN)_2$ and $Hg(PAN)_2$ in ethanol are shown in Figure 6. $Cd(PAN)_2$ displays a maximum at 22000 cm^{-1} (λ =

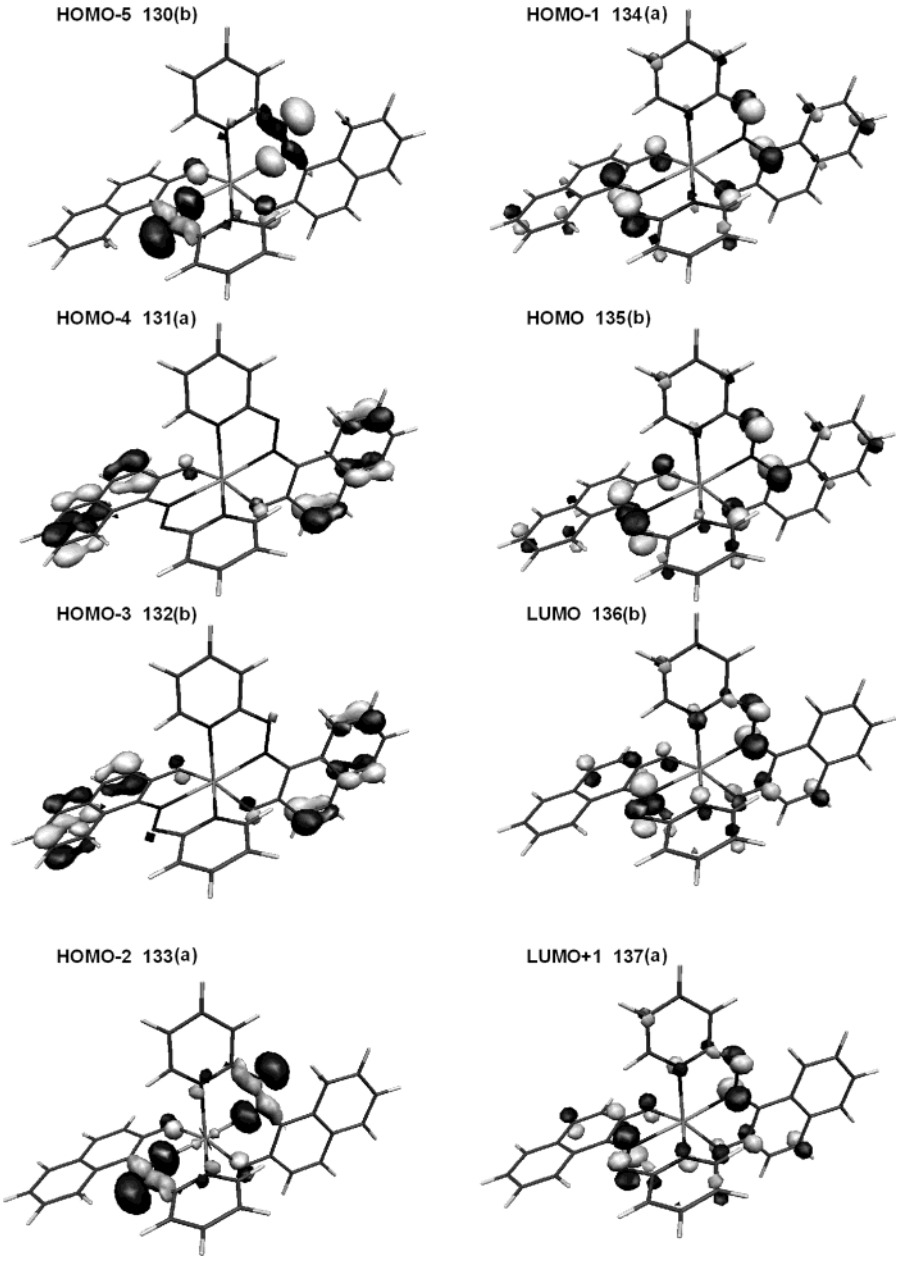

Figure 4. Diagrams of the frontier orbitals of $Cd(PAN)_2$ and $Hg(PAN)_2$.

450 nm), with a shoulder at ca. 24400 cm^{-1} ($\lambda = 410$ nm), and $Hg(PAN)_2$ a band at 21700 cm^{-1} ($\lambda = 460$ nm), with a shoulder at ca. 23800 cm^{-1} ($\lambda = 420$ nm). These are in good agreement with the predicted transitions, and the main peaks can therefore be attributed to the overlapped $^1A \leftarrow ^1A$ and $^1B \leftarrow ^1A$ π-π^* transitions associated mainly with the PAN^- ligands. The higher energy shoulders are assigned to the second pair of overlapped $^1A \leftarrow ^1A$ and $^1B \leftarrow ^1A$ transitions predicted around 406 nm. That the absorption bands for the Hg(II) complex are at somewhat lower energy than those for the Cd(II) complex is in accordance with the calculated transitions listed in Table 4.

RR Spectra. The RR spectra of $Cd(PAN)_2$ and $Hg(PAN)_2$, excited at 457.9, 488.0, and 514.5 nm are presented in Figures 7 and 8, respectively. These spectra are dominated by bands associated with the PAN^- ligands, in accordance with the mainly π-π^* nature of the resonant electronic transition. Strong luminescence occurs for $Cd(PAN)_2$ with 514.5 nm excitation and for $Hg(PAN)_2$ with all excitation wavelengths. Band positions and assignments are listed in Tables 6 and 7 for $Cd(PAN)_2$ and $Hg(PAN)_2$, respectively. For excitation throughout the region of the main absorption band it is found that, for both complexes, the three strongest bands are those at 1200, 1396, and 1484 cm^{-1}. The 1484 cm^{-1} band is attributed to a mode involving CO stretching and in-plane deformation of the naphthalene CH groups, with only small contributions from naphthalene ring stretching. Both the 1200 and 1396 cm^{-1} bands involve naphthalene ring stretching. This is surprising in that the resonant electronic transition appears to involve very little alteration of electron density on the naphthalene rings but does significantly involve the azo group. The NN stretching coordinate contributes to bands at 1256, 1312, and 1336 cm^{-1} but these are only weak to medium intensity bands, whereas the NN stretch is by far the strongest band in the RR spectra of a wide range of aromatic azo compounds.[22] This is undoubtedly connected with the long NN distance, and low band wavenumber, consistent with a NN bond order intermediate between 1 and 2. By contrast, in azobenzene derivatives with a NN bond order of 2 the ν(NN) band is typically found at ca. 1400 cm^{-1}.

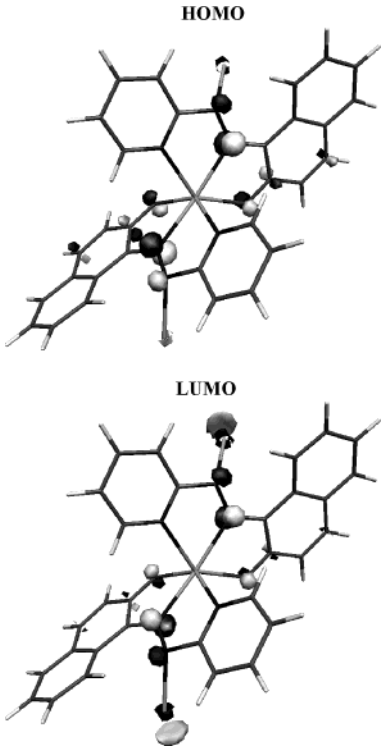

Figure 5. Diagrams of the HOMO and LUMO of $Cd(PAN)_2$ interacting with silver atoms.

TABLE 5: Calculated Electronic Transitions for $Cd(PAN)_2$ Interacting with Silver Atoms, Correlated with the Transitions Calculated for the Free Complex

	$Cd(PAN)_2\cdots 2Ag$			$Cd(PAN)_2$		
no.		λ/nm	f	no.	λ/nm	f
1	$^1B\leftarrow{}^1A$	5412.25	0.0247			
2	$^1A\leftarrow{}^1A$	1625.06	0.0026			
3	$^1B\leftarrow{}^1A$	1621.65	0.0711			
4	$^1B\leftarrow{}^1A$	707.58	0.0227	2	555.47	0.0021
5	$^1A\leftarrow{}^1A$	696.80	0.0007			
6	$^1B\leftarrow{}^1A$	652.17	0.0276	2	555.47	0.0021
7	$^1A\leftarrow{}^1A$	644.82	0.0051	1	555.85	0.0018
8	$^1A\leftarrow{}^1A$	561.40	0.0151	1	555.85	0.0018
9	$^1B\leftarrow{}^1A$	561.05	0.0081			
10	$^1A\leftarrow{}^1A$	530.35	0.0673	5	478.12	0.3035
11	$^1B\leftarrow{}^1A$	521.74	0.0544	6	475.58	0.4642
12	$^1B\leftarrow{}^1A$	520.91	0.2195	6	475.58	0.4642
13	$^1A\leftarrow{}^1A$	520.24	0.0102	5	478.12	0.3035
14	$^1A\leftarrow{}^1A$	491.56	0.0077			
15	$^1B\leftarrow{}^1A$	486.53	0.0090			
16	$^1B\leftarrow{}^1A$	451.71	0.0477			
17	$^1B\leftarrow{}^1A$	447.70	0.0945			
18	$^1A\leftarrow{}^1A$	446.29	0.0200			
19	$^1A\leftarrow{}^1A$	440.08	0.0243	7	405.85	0.0010
20	$^1B\leftarrow{}^1A$	426.27	0.0066	8	405.85	0.0581

Most other bands in the RR spectra are associated with stretching and deformation of the naphthalene rings, although there are some bands which are attributable to vibrations of the pyridine rings, although only two of these display appreciable intensity. Those are the bands at 984 cm^{-1} (pyridine ring breathing and naphthalene ring stretch) and 460 cm^{-1} (pyridine out-of-plane ring deformation). The only metal−ligand vibration observed in the RR spectra is the one at 220 cm^{-1}, which has a contribution from metal−oxygen stretching.

SERRS Spectra. The SERRS spectra of $Cd(PAN)_2$ and $Hg(PAN)_2$ are shown in Figures 9 and 10, respectively, as a function of excitation wavelength, together with the corresponding RR spectra excited at 514.5 nm. Band positions and

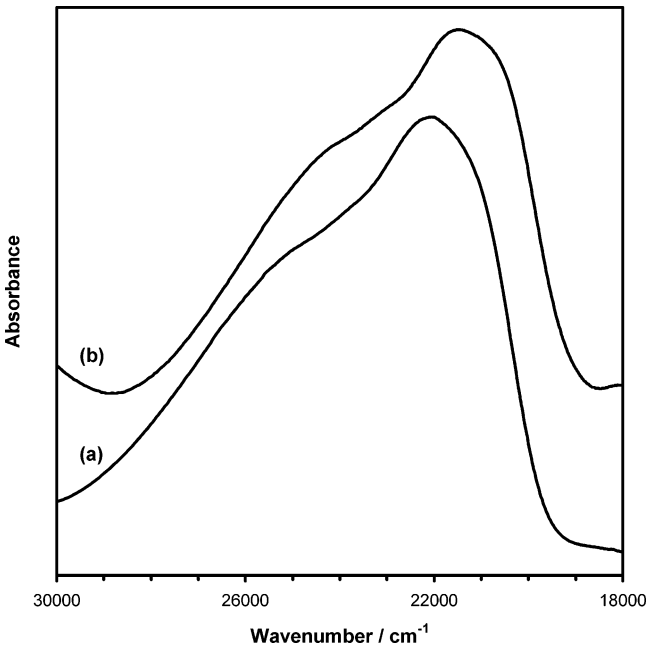

Figure 6. Electronic absorption spectra of (a) 10^{-5} mol dm^{-3} $Cd(PAN)_2$ in ethanol and (b) 10^{-5} mol dm^{-3} $Hg(PAN)_2$ in ethanol.

assignments are listed in Tables 6 and 7, respectively. SERRS spectra were obtained from silver sol samples containing 5×10^{-6} mol dm^{-3} of either $Cd(PAN)_2$ $Hg(PAN)_2$ and 5×10^{-3} mol dm^{-3} KCl. The relative intensity distribution is significantly modified in the SERRS spectra; the strongest bands are now those at 1452, 1338, and 1228 cm^{-1}. The 1452 cm^{-1} band, which corresponds to the weak 1472 cm^{-1} band in the RR spectra, is assigned to a vibration of the pyridine rings involving ring stretching and deformation and in-plane CH deformation. Both the 1338 and 1228 cm^{-1} bands correspond to vibrations involving contributions from NN stretching, although the 1338 cm^{-1} band is also associated with pyridine ring in-plane deformation. The very strong band at 1396 cm^{-1} in the RR spectrum has lost intensity and shifted to 1360 cm^{-1}. Likewise, the other very strong RR bands (1484 and 1200 cm^{-1}) are shifted and weakened in the SERRS spectra. All of these alterations in band positions and intensities can be interpreted in terms of the chemical mechanism of SERRS. In particular, the altered band positions are in accord with the predictions listed in Table 3 for $Cd(PAN)_2$ interacting with silver atoms through the azo α-nitrogen atoms. Calculations on these complexes interacting with either two Ag^+ ions or one Ag^+ ion and one neutral Ag atom did not give a satisfactory fit to the observed band shifts in the SERRS spectra.

The excitation wavelength dependence of SERRS of the $M(PAN)_2$ complexes adsorbed on silver sol was studied using a variety of Ar^+ laser lines. Although these samples had been prepared by mixing silver sol with ethanolic solutions of the complexes, no Raman bands of ethanol could be detected in the SERRS spectra. For this reason it was necessary to compare the variation of band intensities without an internal standard. Hence the 1608 cm^{-1} band of the $M(PAN)_2$ of the complexes was employed as an intensity standard, since this band appears to show the least change in position upon adsorption for all three complexes.

It is apparent that on, adsorption, most bands become more intense with respect to the 1608 cm^{-1} band with increasing excitation wavelength, i.e., as excitation is tuned toward the surface plasmon resonance of the partially aggregated silver nanoparticles. For excitation closest to the surface plasmon

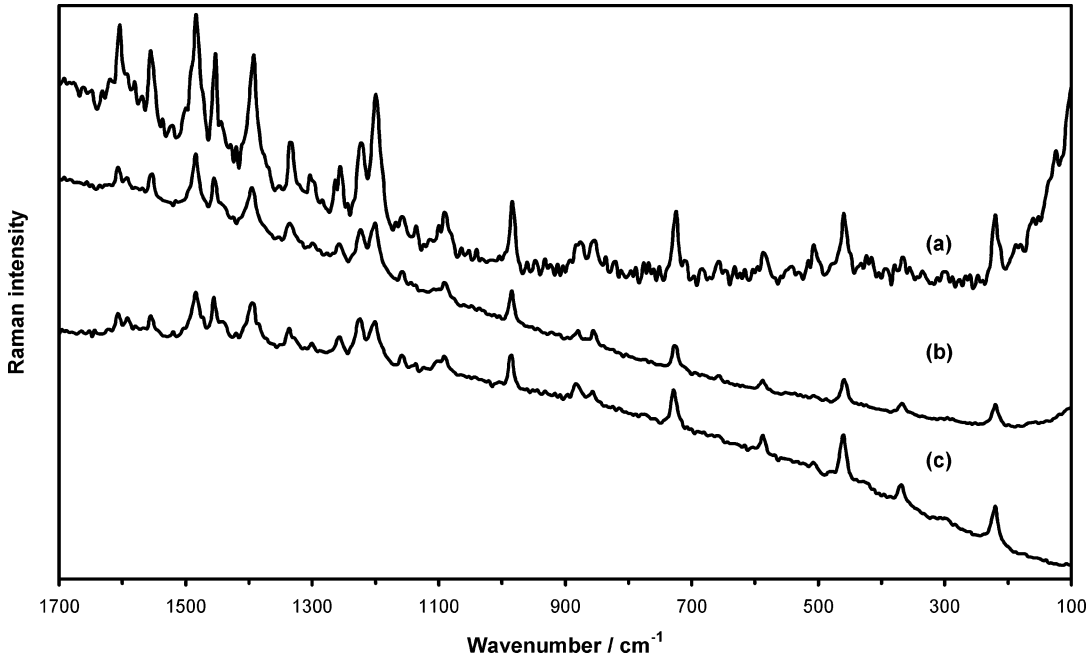

Figure 7. RR spectra of 10^{-3} mol dm^{-3} Cd(PAN)$_2$ in ethanol, excited at (a) 457.9, (b) 488.0, and (c) 514.5 nm.

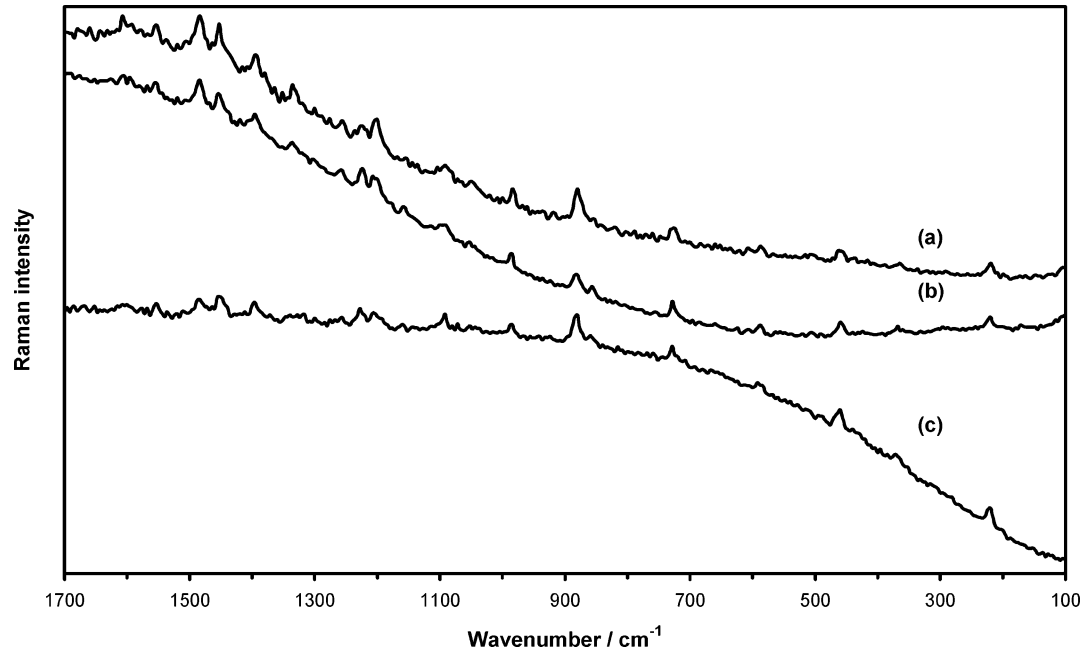

Figure 8. RR spectra of 10^{-3} mol dm^{-3} Hg(PAN)$_2$ in ethanol, excited at (a) 457.9, (b) 488.0, and (c) 514.5 nm.

resonance ($\lambda_0 = 528.7$ nm) the 1228 and 1328 cm^{-1} bands are the most enhanced. These bands, which are assigned to vibrations involving a significant ν(NN) component, display greater enhancement, with respect to the 1608 cm^{-1} band, in the SERRS spectrum than they do in the RR spectrum; this is attributed to a chemical contribution to the surface enhancement, resulting from chemisorption. These experimental observations are consistent with the interaction of surface silver atoms with the azo α-nitrogen atoms of the complex. At shorter wavelengths these bands become weaker, as they do also in the RR spectra excited at shorter wavelengths. It is clear, however, that the high wavenumber bands are generally subject to a greater degree of surface enhancement than the lower wavenumber bands (<900 cm^{-1}). The possible reasons for this are 2-fold: (a) invoking the chemical contribution to SERRS it might be that the normal modes giving rise to the low wavenumber vibrations are less active in the "metal-adsorbate" excited state than they are in the resonant excited state of the free molecule and (b) it may be that in the electromagnetic contribution to the surface enhancement the adsorbate orientation favors a greater degree of enhancement for the high wavenumber vibrations.

Discussion

The SERRS spectra of both complexes show substantial differences in relative band intensities compared with their RR spectra, and many bands are shifted in position. The strongest RR bands for both complexes are associated with naphthalene ring vibrations although these mostly become relatively less intense in the SERRS spectra. The nature of the interaction of these M(PAN)$_2$ complexes with the silver surface is revealed by the differences between their RR and SERRS spectra. These

TABLE 6: Band Wavenumbers and Assignments for the RR and SERRS Spectra of $Cd(PAN)_2$

wavenumber/cm[1]				assignments[a]		
RR		calc	SERRS		calc	
1608	s	1607	1608	m	1606	N_{20}, N_{31}
1592	w	1602	1592	m	1596	S_{8b}
			1564	w	1558	S_{8a}
1556	s	1551	1548	m	1537	N_5, N_6, N_{41}
1520	w	1522	1480	vw,sh	1507	ν(CO), N_{40}
1484	vs	1479	1468	m	1467	ν(CO), δ_{ip}(CH-nap.)
1472	sh	1466	1452	vs	1437	S_{19b}, δ_{ip}(CH-pyr.)
1456	s	1449				N_{20}, δ_{ip}(CH-nap.)
1448	sh	1434	1420	vw	1428	S_{19a}, δ_{ip}(CH-pyr.)
1408	sh	1409				δ_{ip}(CH-nap.)
1396	vs	1380	1360	s	1369	N_{40}, ν(CN)
1375	sh	1358	1376	w		N_3, N_4, N_6
1336	m	1337	1328	vs	1327	ν(NN), S_{14}
1312	w	1317	1304	vw	1298	ν(NN), S_{14}, δ_{ip}(CH-pyr.)
1256	m	1248	S_{12}, ν(CN)			
1256	m	1263	1228	vs	1235	ν(NN), δ_{ip}(CH-nap.)
1224	m	1245	ν(CN)			
1200	s	1225	1212	w	1226	N_{40}, δ_{ip}(CH-nap.)
1184	w	1177	δ_{ip}(CH-nap.)			
1160	w	1160	1160	w	1164	δ_{ip}(CH-pyr.)
1132	w	1144	1140	w	1140	N_{19}, δ_{ip}(CH-nap.)
1112	w	1112	S_{19a}, δ_{ip}(CH-pyr.)			
1092	m	1086	1092	m	1074	N_{24}, N_{32}, N_{36}
1020	m	1013	S_1, S_{12}, δ_{op}(CH-nap.)			
984	s	1002	988	w	1000	S_1, N_{39}, N_{41}
			916	w	899	δ_{op}(CH-nap.)
882	w	890				N_{24}, δ(CNN)
856	w	853	860	w	855	S_1, N_{24}, ν(C6N11)
			760	m	756	S_4, δ_{op}(CH-pyr.)
728	s	731	736	w	728	N_6, N_{36}
656	w	645	660	w	655	S_{6a}, N_{35}
			645	w	645	S_{6a}, S_{6b}
588	w	588	584	w	569	N_{47}, δ_{op}(CN), τ(CN), τ(NN)
			568	vw	564	N_{25}
			536	vw	535	S_4, N_{16}, N_{27}, δ_{op}(CN)
508	w	515	508	vw	520	N_{23}, δ_{ip}(CN), δ_{ip}(CO)
460	s	440	448	m	436	S_{16a}, S_{16b}
			382	vw	395	N_{12}, N_{16}, τ(CN), δ_{op}(AgN)
			320	vw	336	N_{35}, δ_{ip}(CN)
220	s	217	220	vw	226	δ_{ip}(CN), δ(CNN), ν(CdO)

data indicate that there is chemisorption involving bonding to surface silver atoms through the azo group α-nitrogen atom, which is supported by B3-LYP/LanL2DZ calculations. We therefore propose the structure shown in Figure 11 for the adsorbed molecule. Molecular models involving interaction with either two Ag^+ ions or one Ag^+ ion and one neutral Ag atom proved not to account for the observed band shifts. This is possibly surprising, given that it has been suggested that there may be positively charged adsorption sites or adatoms on the surface of Ag nanoparticles. It is likely in the present case that either (i) because the Ag sols have been prepared by reduction with $NaBH_4$ the Ag particles remain in a reducing environment where the formation of Ag^+ ions is unfavorable or (ii) that adsorption is preferred at neutral Ag sites. The latter might be the case as coordination of the ligands to a metal cation in the complex, draws charge away from the azo group α-nitrogen atom.

Surface selection rules based upon the electromagnetic SERS mechanism[17] often provide the key to the determination of adsorbate geometry. For the $M(PAN)_2$ complexes these rules dictate that, for a perpendicular edge-on orientation of a ligand with respect to the silver surface, the electromagnetic enhancement would be greater for ring stretching vibrations and in-plane deformations, which involve motion perpendicular to the surface, than for out-of-plane deformations. The exact opposite would be true for a flat-on parallel adsorbate orientation. However, only totally symmetric vibrations appear in the SERRS spectra of these complexes, as a consequence of RR scattering in the A-term regime.[16] For totally symmetric modes the surface selection rules are not usually able to predict which modes are the most electromagnetically enhanced because we do not know the relative magnitudes of the transition polarizability components α_{xx}, α_{yy}, and α_{zz} for each mode. Although there are several published reports of adsorbate orientations determined from comparison of relative intensities of totally symmetric modes alone, there is no theoretical basis for these and any conclusions drawn must be regarded as unsound.

Although the SERRS data could be interpreted in terms of either a parallel or perpendicular adsorbate orientation the former is more likely on the grounds that a perpendicular orientation would require awkward steric interaction of the edges of the naphthalene and pyridine rings with the silver surface. In the parallel flat-on orientation the large enhancement noted for the high wavenumber bands would be a consequence of these totally symmetric ring stretches being the modes most enhanced by a contribution from resonance with silver-π^* charge transfer, on the assumption that such a charge transfer would lead to ring expansion. Hence the Raman band intensity behavior must be controlled by a chemical contribution to the surface enhancement. This orientation would allow interaction of silver surface with the azo α-nitrogen atoms on both ligands and is consistent with the observed spectra.

Comparison of the RR and SERRS spectra leads to an estimated surface enhancement of ca. 10^4 for the $M(PAN)_2$

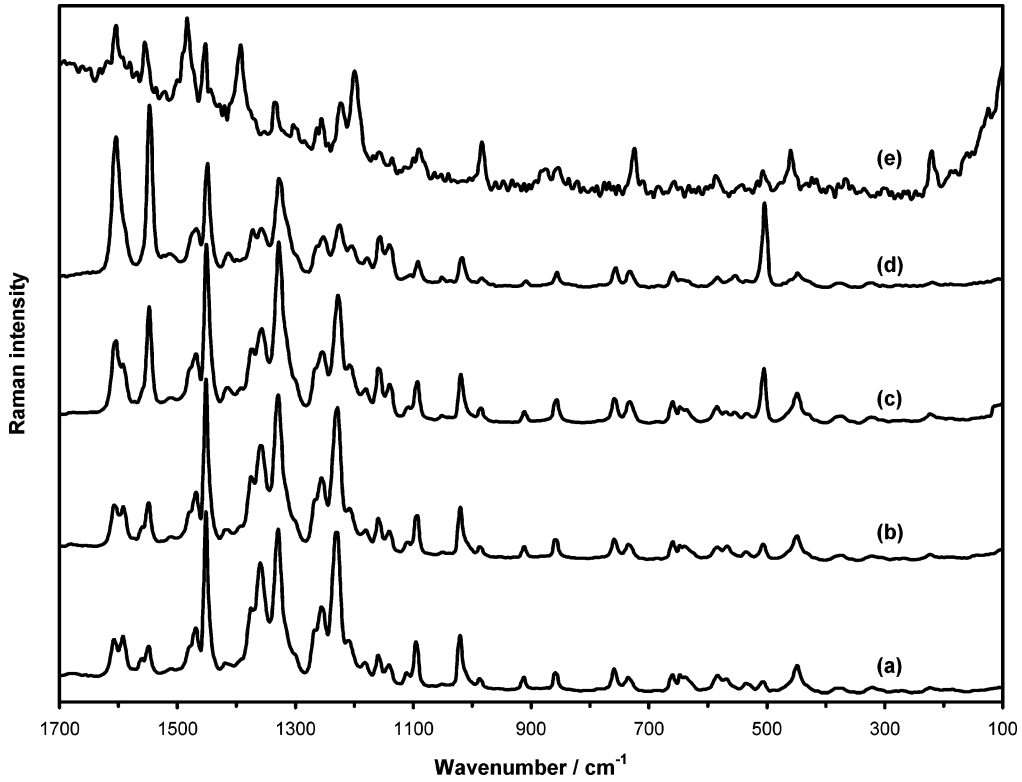

Figure 9. SERRS spectra of 5×10^{-6} mol dm^{-3} $Cd(PAN)_2$, excited at (a) 457.9, (b) 488.0, (c) 514.5 nm, and (d) 528.7 nm, and (e) the RR spectrum of 10^{-3} mol dm^{-3} $Cd(PAN)_2$ in $CHCl_3$ at 514.5 nm excitation.

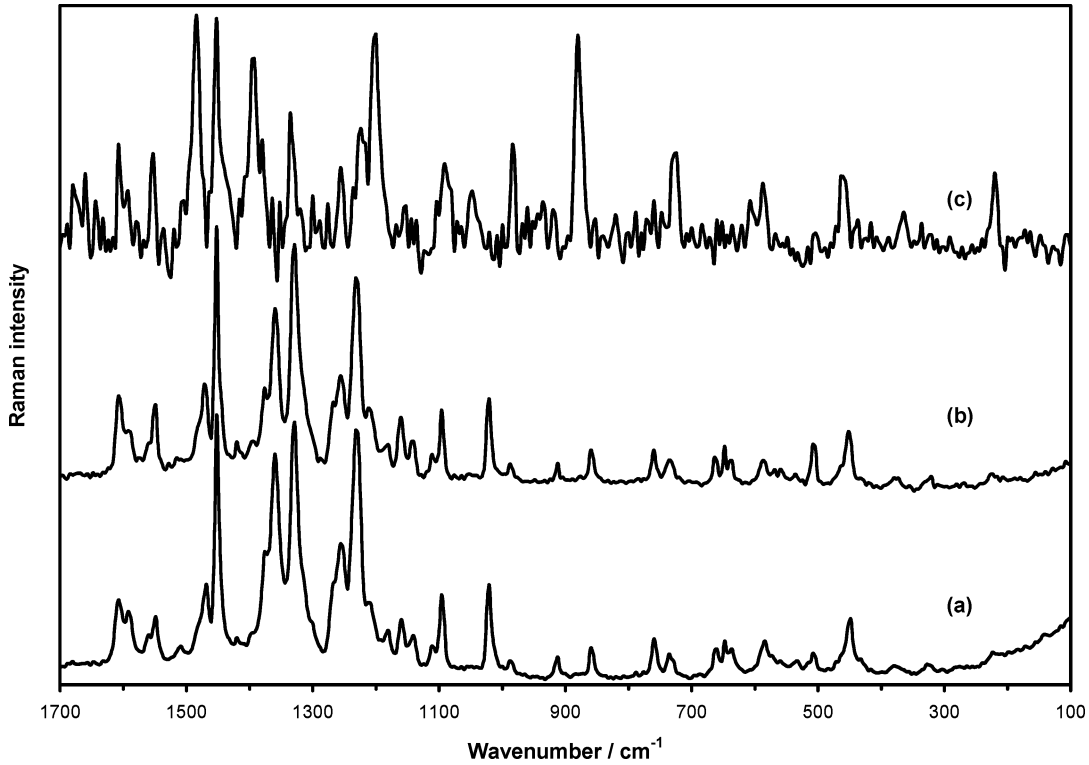

Figure 10. SERRS spectra of 5×10^{-6} mol dm^{-3} $Hg(PAN)_2$, excited at (a) 514.5 and (b) 457.9 nm and (c) the baseline-corrected RR spectrum of 10^{-3} mol dm^{-3} $Hg(PAN)_2$ in $CHCl_3$ at 514.5 nm excitation.

complexes adsorbed on silver colloid. This is small compared with the enhancement factor of 10^6 obtained for many other adsorbates, but similar behavior has been reported in other SERRS studies.[23,24] A reduction in surface enhancement can be explained in terms of a broadening of adsorbate electronic energy level as a consequence of chemisorption on silver. Interaction with the surface provides alternative pathways for vibrational relaxation, shortening the lifetime of the resonant excited state. This in turn increases the homogeneous broadening of adsorbate electronic energy levels, thereby reducing the Raman intensity enhancement. This explanation is supported by the knowledge that a reduced surface enhancement is found when the adsorbate is chemisorbed but not when there is only physisorption.[4]

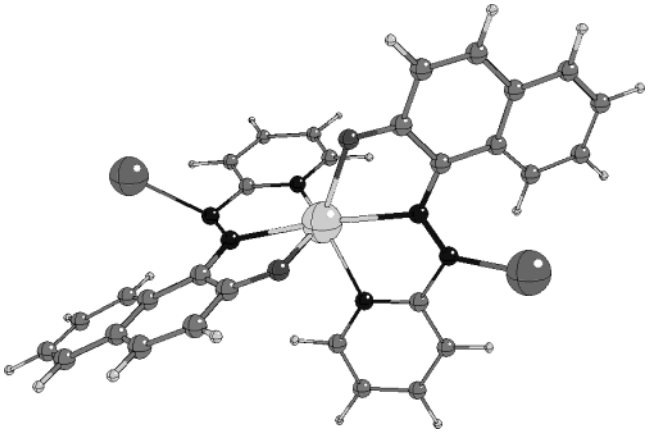

Figure 11. The structure of $M(PAN)_2$ complexes adsorbed on silver.

TABLE 7: Band Wavenumbers and Assignments for the RR and SERRS Spectra of $Hg(PAN)_2$

	wavenumber/cm[1]			assignments[a]		
RR		calc	SERRS		calc	
1608	m	1607	1608	m	1606	N_{20}, N_{31}
1592	w	1601	1592	m	1596	S_{8b}
1580	w	1568	1551	m	1548	S_{8a}
1552	m	1551				N_5, N_6, N_{41}
1484	vs	1478	1468	m	1465	N_3, ν(CO), δ_{ip}(CH-nap.)
1452	vs	1447	1452	vs	1437	N_{20}, δ_{ip}(CH-nap.)
1396	s	1377	1360	vs	1370	N_{39}, ν(CN)
1328	s	1339	1328	vs	1331	ν(NN), S_{14}
1300	w	1295				S_{14}, δ_{ip}(CH-pyr.)
1260	w	1262	1228	vs	1234	ν(NN), δ_{ip}(CH-nap.)
			1256	m	1251	S_{12}, ν(CN)
1228	m	1244				N_{32}, ν(CN), δ_{ip}(CH-nap.)
1208	vs	1225	1208	w	1226	N_{40}, δ_{ip}(CH-nap.)
1160	w	1166	1160	w	1164	δ_{ip}(CH-nap.)
			1140	w	1142	N_{19}, δ_{ip}(CH-nap.)
1092	m	1085	1096	m	1071	N_{24}, N_{32}, N_{36}
			1020	m	1012	S_{12}, δ_{op}(CH-nap.)
984	m	1000	988	w	997	S_1, N_{39}, N_{41}
860	vs	853	860	w	855	S_1, N_{24}, ν(C6N11)
			760	m	752	S_4, δ_{op}(CH-pyr.)
728	m	730	736	w	742	N_6, N_{36}
668	w	655	668	w	655	S_{6a}, N_{35}
628	m	644	648	w	643	S_{6a}, S_{6b}
608	vw	615	608	w	618	S_{6b}, N_{44}, δ_{ip}(CO)
592	vw	588	584	w	570	N_{47}, δ_{op}(CN), τ(NN)
516	w	519	508	w	533	S_4, S_{16a}, N_{47}, δ_{op}(CN)
			460	m	489	S_{6b},N_{23}, δ_{ip}(CO)
436	vw	437	448	m	439	S_{16a}, S_{16}, N_{12}, N_{47}
372	w	379	380	w	388	N_{12}, N_{47}, τ(CN)
316	vw	308	320	w	327	S_{16a}, S_{16}, τ(CN)
			296	vw	289	N_{35}, δ_{ip}(CN)
220	m	214	224	w	222	δ_{ip}(CN), δ(CNN), ν(HgO)

The results show a clear difference in dependence on excitation wavelength for the SERRS and RR spectra. Such behavior cannot be interpreted in terms of the electromagnetic SERS mechanism alone. There must also be a chemical contribution, and, in particular, silver$\rightarrow\pi^*$ charge transfer is predicted to result in a perturbation of the electronic excited state energies of the complexes as well as an alteration of their excited-state molecular geometries. Both of these effects may cause the RR spectra of the free complexes and the SERRS spectra of the adsorbed species to exhibit markedly different dependence on excitation wavelength. Hence there is clear evidence for interaction of the complexes with the silver surface and for the modification of their molecular electronic energy levels upon chemisorption, which is clearly supported by ab initio calculations of the molecular geometries, Raman spectra and electronic excited states for the free complexes, and the changes attendant upon interaction with silver atoms.

References and Notes

(1) Aroca, R. In *Vibrational Spectroscopy and Structure*; Durig, J. R., Ed.; Elsevier: Amsterdam, 1991; Vol. 19, p 55.

(2) Campion, A.; Kambhampati, P. *Chem. Soc. Rev.* **1998**, *27*, 241.

(3) Hildebrandt, P.; Stockburger, M. *J. Phys. Chem.* **1984**, *88*, 5935.

(4) Dines, T. J.; Peacock, R. D. *J. Chem. Soc., Faraday Trans. 1* **1988**, *84*, 3445.

(5) Long, M. E.; Trotter, P. J. *Appl. Spectrosc.* **1981**, *35*, 289.

(6) Drożdżewski, P. M. *Spectrochim. Acta* **1985**, *41A*, 1035.

(7) Drożdżewski, P. M. *J. Raman Spectrosc.* **1988**, *19*, 111.

(8) Dines, T. J.; Wu, H. *J. Chem. Soc., Faraday Trans.* **1995**, *91*, 463.

(9) Creighton, J. A.; Blatchford, C. G.; Albrecht, M. G. *J. Chem. Soc., Faraday Trans. 2* **1979**, *75*, 790.

(10) Adams, H.; Bucknall, R. M.; Fenton, D. E.; Garcia, M.; Oakes, J. *Polyhedron* **1998**, *17*, 4169

(11) *Gaussian 98, Revision A.5*, Frisch, M. J.; Trucks, G. W.; Schlegel, H. B.; Scuseria, G. E.; Robb, M. A.; Cheeseman, J. R.; Zakrzewski, V. G.; Montgomery, J. A., Jr.; Stratmann, R. E.; Burant, J. C.; Dapprich, S.; Millam, J. M.; Daniels, A. D.; Kudin, K. N.; Strain, M. C.; Farkas, O.; Tomasi, J.; Barone, V.; Cossi, M.; Cammi, R.; Mennucci, B.; Pomelli, C.; Adamo, C.; Clifford, S.; Ochterski, J.; Petersson, G. A.; Ayala, P. Y.; Cui, Q.; Morokuma, K.; Malick, D. K.; Rabuck, A. D.; Raghavachari, K.; Foresman, J. B.; Cioslowski, J.; Ortiz, J. V.; Stefanov, B. B.; Liu, G.; Liashenko, A.; Piskorz, P.; Komaromi, I.; Gomperts, R.; Martin, R. L.; Fox, D. J.; Keith, T.; Al_Laham, M. A.; Peng, C. Y.; Nanayakkara, A.; Gonzalez, C.; Challacombe, M.; Gill, P. M. W.; Johnson, B.; Chen, W.; Wong, M. W.; Andres, J. L.; Gonzalez, C.; Head_Gordon, M.; Replogle, E. S.; Pople, J. A.; Gaussian, Inc.; Pittsburgh, PA, 1998.

(12) Becke, A. D. *J. Chem. Phys.* **1993**, *98*, 5648.

(13) Lee, C.; Yang W.; Parr, R. G. *Phys. Rev. B* **1988**, *37*, 785.

(14) Dunning, T. H. Jr.; Hay, P. J. *Modern Theoretical Chemistry*; Schaefer, H. F. III, Ed.; Plenum: New York; 1976; Vol. 3, p 1.

(15) Hay, P. J.; Wadt, W. R. *J. Chem. Phys.* **1985**, *82*, 270, 284, and 299.

(16) Clark, R. J. H.; Dines, T. J. *Angew. Chem., Int. Ed. Engl.* **1986**, *25*, 131.

(17) Creighton, J. A. *Advances in Spectroscopy;* Clark, R. J. H., Hester, R. E., Eds.; J. Wiley & Sons: Chichester, 1988; Vol. 16.

(18) *18.Schachtschneider, J. A. Vibrational Analysis of Polyatomic Molecules*; Parts V and VI; Technical Report Nos. 231 and 57; Shell Development Co.: Houston TX, 1964 and 1965.

(19) Pulay, P.; Fogarasi, G.; Pang, F.; Boggs J. E.; Vargha, A. *J. Am. Chem. Soc.* **1983**, *105*, 7037.

(20) Varsányi, G. *Vibrational Spectra of Benzene Derivatives*; Academic Press: New York, 1969.

(21) Casida, M. E.; Jamorski, C.; Casida, K. C.; Salahub, D. E. *J. Chem. Phys.* **1998**, *108*, 4439.

(22) Machida, K. *Raman Spectroscopy: Sixty Years On, Vibrational Spectra and Structure*; Durig, J. R., Ed.; Elsevier: Amsterdam, 1989; Vol. 17A, p 421.

(23) Siiman, O.; Lepp, A. *J. Phys. Chem.* **1984**, ***88***, 2641.

(24) Weitz, D. A.; Garoff, Gersten, J. L.; Nitzan, A. *J. Chem. Phys.* **1983**, *78*, 5324.